

DIGITIZED NONLINEAR BEAM AND WAVE INTERACTION THEORY OF TRAVELING WAVE TUBE AMPLIFIERS

Weifeng Peng¹, Yulu Hu^{1, *}, Zan Cao², and Zhonghai Yang¹

¹National Key Laboratory of Science and Technology on Vacuum Electronics, University of Electronic Science and Technology of China, Chengdu 610054, China

²China Electronics Standardization Institute, Beijing 100007, China

Abstract—To simulate the beam and wave interaction (BWI) of various types of traveling wave tube amplifiers (TWTAs), a digitized nonlinear theory has been developed with two features. First, the digitized RF field profiles obtained from electromagnetic simulation software are applied to replace the analytical RF field profiles in TWTAs. Second, the relationship of energy conservation between the beam and RF fields is used to derive the RF field equations. Based on this nonlinear theory, one-dimensional (1-D) code has been constructed to predict the performances of TWTAs. Comparisons between the simulations and the experimental results for three types of TWTAs, i.e., a K-band helix TWTA, a V-band coupled cavity (CC) TWTA and a W-band folded waveguide (FWG) TWTA, are discussed to prove this nonlinear theory.

1. INTRODUCTION

Traveling wave tube amplifiers (TWTAs) are important microwave devices widely used in radar, electronic warfare and communication systems [1, 2]. As demand increases for higher frequency and higher power, better performing traditional devices, such as helix TWTAs and coupled cavity (CC) TWTAs are required, while new types of TWTAs, such as folded waveguide (FWG) TWTAs have also been developed. As a result, nonlinear theories for simulating the beam and wave interaction (BWI) of these TWTAs are in demand.

Received 7 December 2012, Accepted 28 December 2012, Scheduled 4 January 2013

* Corresponding author: Yulu Hu (yulu@uestc.edu.cn).

Many nonlinear BWI theories for helix and CC TWTAs have been developed since Pierce and Rowe et al. [3, 4]. Over the past decades, CHRISTINE [5–7], GATOR [8–10] and SUNRAY [11] theories have been effectively applied to helix and CC TWTAs [12–14]. LSCEX [15–17] and TESLA [18–20] have also been applied to CC TWTAs. Characteristics of helix and CC TWTAs are significantly improved by these nonlinear theories. But for the FWG TWTAs, no nonlinear BWI theory has been reported yet. Instead, three dimensional (3-D) particle-in-cell (PIC) software such as MAGIC [21], can be employed to simulate the FWG TWTAs in time domain, but the cost is huge for the large quantity of computing time for practical tube designs.

In this paper, to simulate the BWI of various types of TWTAs in a unified way, a digitized nonlinear theory is developed with two features. First, with the digitized RF fields in a single period obtained from the electromagnetic simulation software (such as HFSS [22]), the RF field profile in the whole tube can be provided by means of the Floquet theorem. Second, the RF field equations are developed from the Law of Energy Conservation. On combing the RF field equations, the Lorentz equations and the space charge (SC) field equations, a nonlinear BWI theory in frequency domain is proposed. Performance of a K-band helix TWTA, a V-band coupled cavity (CC) TWTA [23] and a W-band folded waveguide (FWG) TWTA [24] shown in Figure 1 has been accurately predicted by the one-dimensional (1-D) parametric code based on this digitized nonlinear theory. Compared with the PIC code, this parametric code can save substantial computing sources. For example, the time and memory costs for a single calculation by this 1-D code in a personal computer (CPU 2.4 GHz, Memory 2 GB) are typically less than 10 min and 20 MB, respectively.

The organization of this paper is as follows. In Section 2, a nonlinear BWI theory is constructed by the combination of the RF field equations, the SC field equations and the dynamic equations.

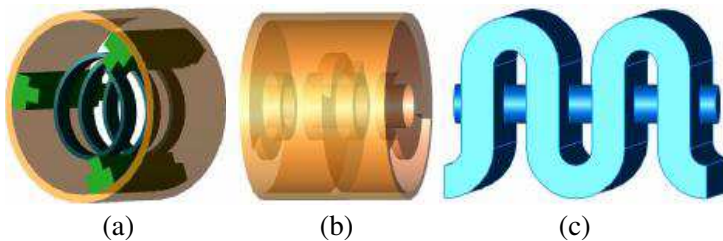


Figure 1. Schematic for the slow wave structures of (a) helix, (b) CC, and (c) FWG TWTAs.

In Section 3, the helix, CC and FWG TWTAs (shown in Figure 1) simulations are compared with test results. The conclusion of this paper is in Section 4.

2. THE NONLINEAR BWI THEORY

The RF fields acting on the electron beam propagating in the slow wave structure (SWS) of a TWTA can be represented in the form of a product as

$$\mathbf{E}_{rf}(\mathbf{x}, t) = \sum_n \mathbf{E}_{rf,n}(\mathbf{x}, t) = \sum_n [f_n(z) \mathbf{e}_n(\mathbf{x}) e^{-i\omega_n t}] \quad (1)$$

for the RF electric field, and

$$\mathbf{H}_{rf}(\mathbf{x}, t) = \sum_n \mathbf{H}_{rf,n}(\mathbf{x}, t) = \sum_n [f_n(z) \mathbf{h}_n(\mathbf{x}) e^{-i\omega_n t}] \quad (2)$$

for the RF magnetic field, where

subscript n is the RF signal number, and ω_n is the angular frequency;

$\mathbf{e}_n(\mathbf{x})$ and $\mathbf{h}_n(\mathbf{x})$ are the RF field profiles without electron beam loaded;

$f_n(z)$ is the complex amplitude varying along the z axial.

It is seen from (1) and (2) that two points need be considered to construct the RF field equations. They are 1) expressions of $\mathbf{e}_n(\mathbf{x})$ and $\mathbf{h}_n(\mathbf{x})$, and 2) the evolution of $f_n(z)$. Both of the two points will be discussed.

2.1. The RF Field Profiles

The RF field profiles $\mathbf{e}_n(\mathbf{x})$ and $\mathbf{h}_n(\mathbf{x})$ can be generally expressed by the Floquet theorem as

$$\mathbf{e}_n(\mathbf{x}) = \mathbf{e}_n(\mathbf{x}_\perp, z) = \boldsymbol{\varsigma}_n(\mathbf{x}_\perp, z_0) e^{im\varphi_n} \quad z_0 \in [0, \lambda_h) \quad (3)$$

$$\mathbf{h}_n(\mathbf{x}) = \mathbf{h}_n(\mathbf{x}_\perp, z) = \boldsymbol{\xi}_n(\mathbf{x}_\perp, z_0) e^{im\varphi_n} \quad z_0 \in [0, \lambda_h) \quad (4)$$

where

subscript \perp stands for the transverse components;

m is the period number equal to the integer of z/λ_h , and λ_h is the axial period length;

φ_n is the phase shift for the n th RF signal in one period;

$\boldsymbol{\varsigma}_n(\mathbf{x}_\perp, z_0)$ and $\boldsymbol{\xi}_n(\mathbf{x}_\perp, z_0)$ are electric and magnetic RF field profile in a single period, respectively.

Because of the variety and complexity of the SWSs, considerable effort has been concentrated on acquiring the analytical $\mathbf{e}_n(\mathbf{x})$ and $\mathbf{h}_n(\mathbf{x})$ in different types of TWTAs by equivalent circuit [25] or field theory [26–30] methods. Instead, digitized $\mathbf{e}_n(\mathbf{x})$ and $\mathbf{h}_n(\mathbf{x})$ can be obtained by means of HFSS as follows. Firstly, for different phase shift φ_i , its corresponding frequency ω_i , power $p_{hf,i}$ and digitized RF field profiles $\mathbf{E}_{hf,i}(\mathbf{x}_\perp, z_0)$ and $\mathbf{H}_{hf,i}(\mathbf{x}_\perp, z_0)$ can be obtained by HFSS with operations of “Field Overlays”-“Calculator”-“Export”. Secondly, the digitized $\boldsymbol{\varsigma}_i(\mathbf{x}_\perp, z_0)$ and $\boldsymbol{\xi}_i(\mathbf{x}_\perp, z_0)$ can be calculated by

$$\boldsymbol{\varsigma}_i(\mathbf{x}_\perp, z_0) = \frac{\mathbf{E}_{hf,i}(\mathbf{x}_\perp, z_0)}{\sqrt{p_{hf,i}}}, \quad \boldsymbol{\xi}_i(\mathbf{x}_\perp, z_0) = \frac{\mathbf{H}_{hf,i}(\mathbf{x}_\perp, z_0)}{\sqrt{p_{hf,i}}} \quad (5)$$

Thirdly, for the RF signal with specific frequency ω_n , linear interpolation based on frequencies ω_j and ω_k can be applied as

$$\mathbf{a}_n(\mathbf{x}_\perp, z_0) = \mathbf{a}_j(\mathbf{x}_\perp, z_0) \frac{\omega_k - \omega_n}{\omega_k - \omega_j} + \mathbf{a}_k(\mathbf{x}_\perp, z_0) \frac{\omega_n - \omega_j}{\omega_k - \omega_j} \quad (6)$$

where $\omega_j < \omega_n < \omega_k$, and $\mathbf{a} = \boldsymbol{\varsigma}$, or $\boldsymbol{\xi}$. Lastly, digitized $\mathbf{e}_n(\mathbf{x})$ and $\mathbf{h}_n(\mathbf{x})$ can be obtained by substituting (6) into (3) and (4).

The axial RF electric field profiles $\mathbf{z} \cdot \mathbf{e}_n(\mathbf{x})$ for the helix, the CC and the FWG TWTAs at their center frequencies are shown in Figure 2. It can be seen from Figure 2 that, expressions (3) and (4) are effective in various types of TWTAs. It should be noted that, since $\boldsymbol{\varsigma}_n(\mathbf{x}_\perp, z_0)$ and $\boldsymbol{\xi}_n(\mathbf{x}_\perp, z_0)$ are normalized by $p_{hf,n}^{1/2}$ as

$$\frac{1}{2} \int_0^{\lambda_h} \frac{dz}{\lambda_h} \int_t^{t+T} \frac{dt}{T} \iint_A [\boldsymbol{\varsigma}_n(\mathbf{x}) \times \boldsymbol{\xi}_n^*(\mathbf{x}) + \boldsymbol{\varsigma}_n^*(\mathbf{x}) \times \boldsymbol{\xi}_n(\mathbf{x})] \cdot \mathbf{z} ds = 1 \quad (7)$$

the relationship between the amplitude $f_n(z)$ and the RF power is then given by

$$\begin{aligned} p_n(z) &= \frac{1}{2} \int_z^{z+\lambda_h} \frac{dz}{\lambda_h} \int_t^{t+T} \frac{dt}{T} \iint_A [\mathbf{E}_{rf,n} \times \mathbf{H}_{rf,n}^* + \mathbf{E}_{rf,n}^* \times \mathbf{H}_{rf,n}] \cdot \mathbf{z} ds \\ &= |f_n(z)|^2 \end{aligned} \quad (8)$$

where A is the cross sectional area of the SWS.

It is noted that the RF field profiles $\mathbf{e}_n(\mathbf{x})$ and $\mathbf{h}_n(\mathbf{x})$ contain all of their space harmonic components as

$$\mathbf{e}_n(\mathbf{x}) = \sum_{s=-\infty}^{\infty} \mathbf{e}_{n,s} e^{i(k_{zn} + s2\pi/\lambda_h)z}, \quad \mathbf{h}_n(\mathbf{x}) = \sum_{s=-\infty}^{\infty} \mathbf{h}_{n,s} e^{i(k_{zn} + s2\pi/\lambda_h)z} \quad (9)$$

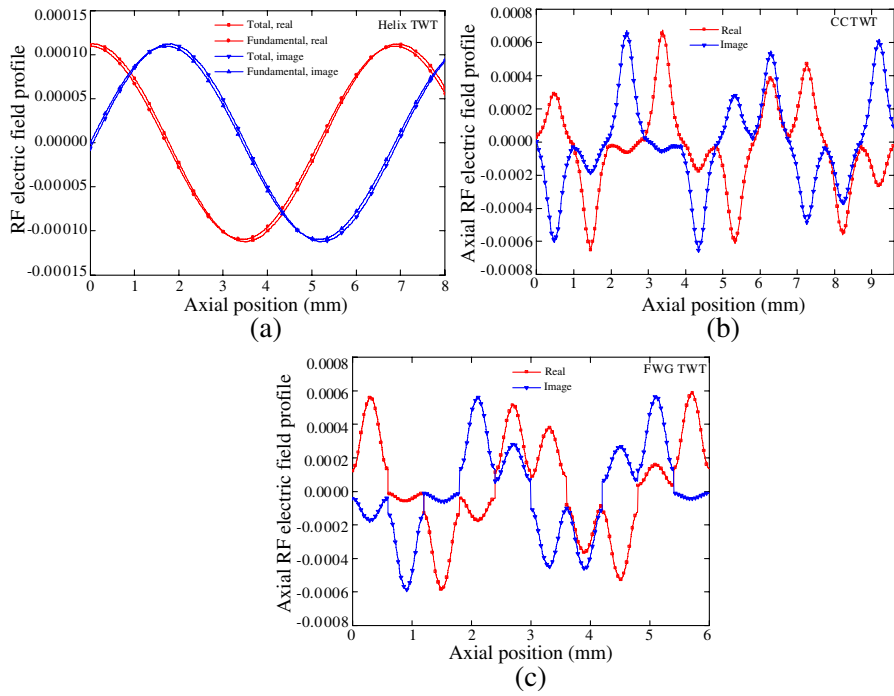


Figure 2. The axial RF electric field profiles for the (a) helix, (b) CC and (c) FWG TWTAs.

where s is the space harmonic number, and $k_{zn} = \varphi_n/\lambda_h$ is the axial wave number of the 0th component. For a helix TWTa, shown in Figure 2(a), its total RF field profile can be described by the 0th space harmonic component as

$$\mathbf{e}_n(\mathbf{x}) = \mathbf{e}_n(\mathbf{x}_\perp, 0) e^{ik_{zn}z} \quad (10)$$

In contrast, for the CC TWTa and for the FWG TWTa (shown in Figures 2(b) and 2(c) respectively), their total RF field profiles contain many space harmonic components. Therefore the RF field profiles in CC or FWG TWTAs can't be represented by expression (10). This distinguishes the general RF field expressions (1) and (2) from the one for the helix TWTAs in the Refs. [5–7].

2.2. The RF Field Equations

On obtaining the RF field profiles, the evolution of the RF field amplitudes, i.e., the RF field equations, can be developed based on the Law of Energy Conservation.

For the k th electron, its dynamical equation is given by

$$\frac{d\gamma_k}{dz} = \frac{1}{m_k c^2} \left\{ \frac{1}{2} q_k \frac{\mathbf{v}_k}{v_{k,z}} \cdot [\mathbf{E}_{rf} + \mathbf{E}_{sc}] dt + c.c. \right\} \quad (11)$$

Therefore, its energy change ΔW_k can be expressed by the mass-energy relation as

$$\Delta W_k = m_k c^2 d\gamma_k = \frac{1}{2} q_k \mathbf{v}_k \cdot [\mathbf{E}_{rf} + \mathbf{E}_{sc}] dt + c.c. \quad (12)$$

where

γ_k , q_k and m_k are the relativistic factor, charge and rest mass of the k th electron, respectively;

c is the speed of light in vacuum, \mathbf{E}_{sc} is the SC field;

coefficient 1/2 and $c.c.$ stand for the real part of the RF fields.

Therefore, the total energy change for the electrons in column V can be given by its integral form as

$$\sum_k \Delta W_k = \frac{dt}{2} \iiint_V \rho \mathbf{v} \cdot \mathbf{E}_{rf} dV + c.c. \quad (\mathbf{x}_k \in V) \quad (13)$$

where $q = \rho dV$ and ρ is the beam charge density and \mathbf{x}_k the position of the k th electron. It should be noted that on the right side of (13) the SC field is not included. Because the SC fields are the Coulomb forces between electrons, the total energy transformation among them is zero.

Particularly, in a TWTA, relationship $dV = A \cdot dz$ can be shown in (13) as

$$\sum_k \Delta W_k = \frac{dz dt}{2} \sum_n \iint_A \mathbf{j} \cdot \mathbf{E}_{rf,n} ds + c.c. \quad (\mathbf{x}_k \in V = A \cdot dz) \quad (14)$$

where $\mathbf{j} = \rho \mathbf{v}$ is the beam current density. On averaging (14) over the time period T and structure period λ_h , expression (14) can be rewritten as

$$\begin{aligned} & \frac{1}{dz dt} \frac{1}{\lambda_h} \int_z^{z+\lambda_h} dz \int_t^{t+T} \frac{dt}{T} \sum_k \Delta W_k \\ &= \frac{1}{2} \sum_n \int_z^{z+\lambda_h} \frac{dz}{\lambda_h} \int_t^{t+T} \frac{dt}{T} \iint_A \mathbf{j} \cdot \mathbf{E}_{rf,n} ds + c.c. \quad (\mathbf{x}_k \in V = A \cdot \lambda_h) \end{aligned} \quad (15)$$

The left side of (15) describes the total amount of the energy change for the electrons in a structure period. According to the Law

of the Energy Conservation between the RF signals and beam, the left side of (15) can be rewritten as

$$\begin{aligned}
 -\frac{1}{dzdt} \left[\frac{1}{\lambda_h} \int_z^{z+\lambda_h} dz \int_t^{t+T} \frac{dt}{T} \sum_k \Delta W_k \right] &= \frac{\Delta W_{rf} + \Delta W_{loss}}{dt dz} \quad (\mathbf{x}_k \in V = A \cdot \lambda_h) \\
 &= \sum_n \left[\frac{dp_n(z)}{dz} + 2\alpha_n(z)p_n(z) \right] \quad (16)
 \end{aligned}$$

where ΔW_{rf} is the energy change of the RF signals, ΔW_{loss} the energy lost in SWS, $\alpha_n(z)$ the attenuation value, and the minus “-” on its left side indicates that the energy is transformed from the electrons to the RF signals, i.e., the electron beam loses energy while the RF power grows during the BWI course. In (15) and (16), the relationship between the RF signals and the beam is given by

$$\begin{aligned}
 \frac{dp_n(z)}{dz} &= \frac{d}{dz} [f_n(z) f_n^*(z)] \\
 &= -\frac{1}{2} \int_z^{z+\lambda_h} \frac{dz}{\lambda_h} \int_t^{t+T} \frac{dt}{T} \iint_A \mathbf{j} \cdot \mathbf{E}_{rf,n} ds - 2\alpha_n(z) p_n(z) + c.c. \quad (17)
 \end{aligned}$$

On substituting expressions (1) and (3) into (17), the RF field equations are given by

$$\begin{aligned}
 &\left[\frac{\partial}{\partial z} + \alpha_n(z) \right] f_n(z) \\
 &= -\frac{1}{2} \int_z^{z+\lambda_h} \frac{dz}{\lambda_h} \int_t^{t+T} \frac{dt}{T} \iint_A \mathbf{j} \cdot \mathbf{e}_n^*(\mathbf{x}_\perp, z_0) e^{-im\varphi_n} e^{i\omega_n t} ds, \quad z_0 \in [0, \lambda_h) \quad (18)
 \end{aligned}$$

Therefore, the transformation relationship between the RF signals and electron beam is characterized well by the Law of Energy Conservation. The corresponding RF field Equations (18) can be confidently applied in different TWTAs.

2.3. The SC Fields

The beam current density can be written in the form of a sum over moving charge particles as

$$\mathbf{j}(\mathbf{x}, t) = \sum_k q_k \mathbf{v}_k \delta[\mathbf{x}_\perp - \mathbf{x}_{\perp k}] \delta[z - z_k] \delta[t - t_k] \quad (19)$$

The axial component of beam current density can be decomposed by the Fourier series as

$$j_z(\mathbf{x}, t) = j_{z0} + \sum_{l=1}^{\infty} \left[j_{z,l}(\mathbf{x}) e^{il\psi} + c.c. \right] \quad (20)$$

where $\psi = \omega_0 t$ is the phase of electrons, ω_0 the greatest common factor of the RF frequencies, l the harmonic number, and the coefficient is

$$j_{z,l}(\mathbf{x}_{\perp}, z) = \frac{1}{T} \sum_{k \in T} q_k \delta[\mathbf{x}_{\perp} - \mathbf{x}_{\perp k}] \delta[z - z_k] e^{-il\psi_k} \quad (21)$$

On substituting AC components in expression (20) into the Helmholtz equations, the SC field equations can be given by

$$\left[\frac{1}{r} \frac{\partial}{\partial r} \left(r \frac{\partial}{\partial r} \right) + \frac{\partial^2}{\partial z^2} + \frac{l^2 \omega_0^2}{c^2} \right] E_{sc,l,z} = \frac{i}{\varepsilon_0 l \omega_0} \left(\frac{\partial^2}{\partial z^2} + \frac{l^2 \omega_0^2}{c^2} \right) j_{z,l} \quad (22)$$

The finite-difference (FD) method is applied to solve the SC field Equation (22) along the axial and radial grids.

Since the RF fields in a TWTA are produced by the charges induced on the surface of a metallic structure surrounding the beam, the SC fields should be fit to the metallic boundary condition. Therefore, the boundary condition for the radial grids is that the SC potential vanishes at the inner radius of beam tunnel, while the periodic boundary conditions are applied for the axial grids.

Ultimately, by combining the governing Equations (11), (18), and (22), the nonlinear theory is constructed and can be numerically integrated over the scale of the SWS to simulate the BWI of a TWTA. Actual SWSs are usually constructed using several sections, including the uniform section with a constant period, the attenuator sections, the sever sections, and the taper sections. Therefore, the TWTA will be modeled by summing the BWI simulations for successive sections.

To theoretically connect all the sections as an actual SWS, information at the end of the current section, such as the RF output power, the speed and position of electrons and the phase of RF signals, will be set as the initial conditions for the next section. In particular, in an attenuator, the attenuation value of the attenuator should be included in $\alpha_n(z)$, while in a sever, the right part of (18) is set to zero.

3. SIMULATION RESULTS AND DISCUSSIONS

Based on this nonlinear BWI theory, 1-D code based on C++ has been constructed. In this 1-D model, electron beam is treated as charge discs moving along axial direction, and the axial electric RF field profile

should be averaged over the transversal area of the beam. It should be noted that in the FD method, though these charge discs have no radial velocity, radial grids are still essential to consider the effect of beam filling ratio on SC fields. The RF field equations and the electron motion equations are stepped by the four-order Runge-Kutta (RK4) method and the SC field equations are solved by finite difference (FD) method. These three TWTAs with SWSs shown in Figure 1 and the BWI parameters, i.e., the frequency, the beam voltage, current and fill ratio listed in Table 1 are modeled by the 1-D code. The simulation and experimental results are shown and discussed in Table 1.

Besides the RF field profiles, the phase speed and attenuation value of a TWTA need to be obtained from HFSS before its BWI simulation. For example, the evolutions of the normalized phase speed and attenuation over the bandwidth of the helix TWTA are calculated and shown in Figure 3.

Table 1. BWI parameters for the three TWTAs.

	Unit	Helix	CC	FWG
Frequency	GHz	24.0–25.0	59.0–64.0	91.5–98.5
Voltage	kV	6.0	19.3	16.5
Current	mA	50.0	73.8	50.0
Fill ratio	—	0.4	0.35	0.3

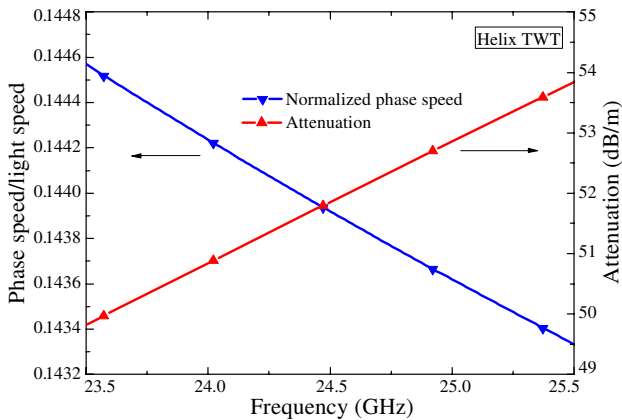


Figure 3. The curves of the normalized phase speed and attenuation of the helix TWTA.

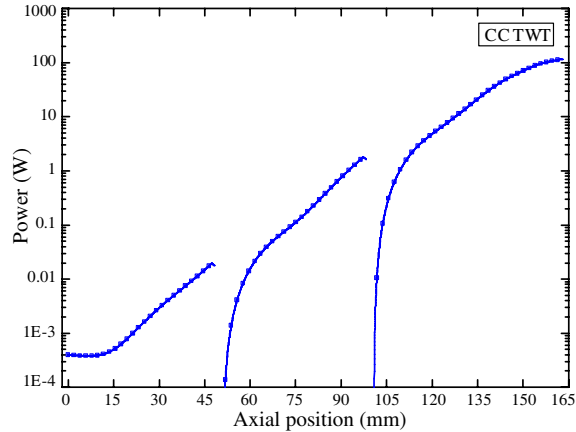


Figure 4. Evolution of power varying with axial position for the CC TWTA at 61.5 GHz.

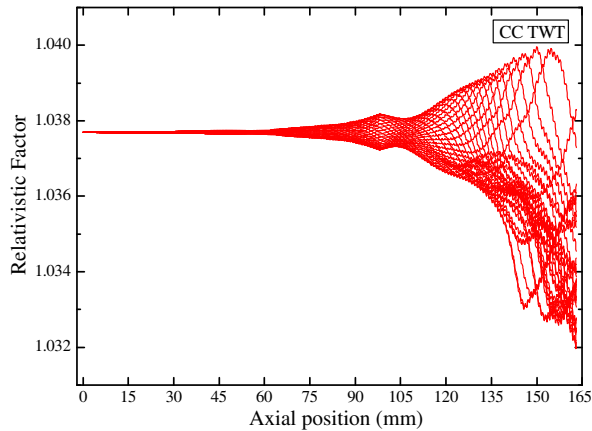


Figure 5. Evolution of electrons' relativistic factor varying with axial position for the CC TWTA at 61.5 GHz.

Figure 4 shows the simulation of the evolution of power with axial position for the center frequency 61.5 GHz of the V-band CC TWTA. The corresponding evolution of its electron axial speed (i.e., the relativistic factor) is shown in Figure 5. It can be seen from Figures 4 and 5 that, as the power growth changes from linear to nonlinear, more electrons decelerate while fewer accelerate, and this accurately characterizes the process of energy transformation from electrons to the RF signals.

Because of nonlinearity, harmonic generation needs to be considered in TWTAs. Therefore, the three-order inter-modulation (3IM) output power for the helix TWTA is shown in Figure 6. In Figure 6, two signals with 100 MHz frequency difference (i.e., 24.5 and 24.6 GHz) and same power of -7.0 dBm are input and the 3IM output power for 24.4, 24.5, 24.6 and 24.7 GHz is shown.

The experimental and simulated results of saturated output power and gain over the bandwidth for the K-band helix, V-band CC and W-band FWG TWTAs are shown as follows.

In Figure 7 for the helix TWTA experimental results, the average value of the output power over the bandwidth is 56.0 W, and the corresponding digitized simulation value is 58.2 W. Meanwhile, both the experimental and digitized simulation saturated gain curves are similar to each other as the relative error averaged over the bandwidth is 0.6%. In Figure 8 the CC TWTA experimental results show that, the average relative error of saturated output power and saturated gain over the bandwidth are 1.2% and 4.3%, respectively.

To compare this digitized nonlinear theory with developed analytical theories, the simulation results by the code for the helix [31] and CC TWTAs [32] are also included in Figures 7 and 8, respectively. For the helix TWTA, it is seen from expression (10) that the RF field profiles from the digitized and analytical theories are equal to each other, so their simulation curves in Figure 7 are also similar. It can be seen in Figure 8 that the simulation results from the two CC TWTA

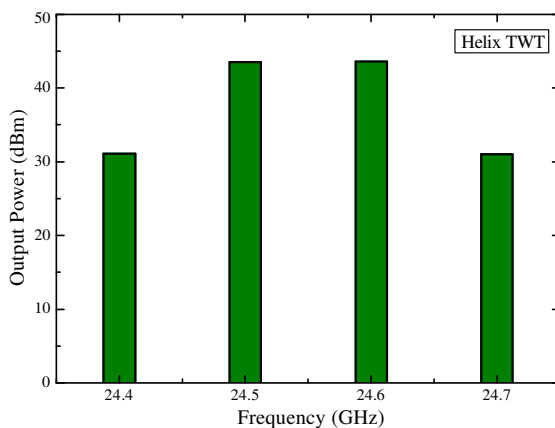


Figure 6. Simulation output spectra of two input tones for the helix TWTA. The input power is -7 dBm and the modulation frequency is 100.0 MHz.

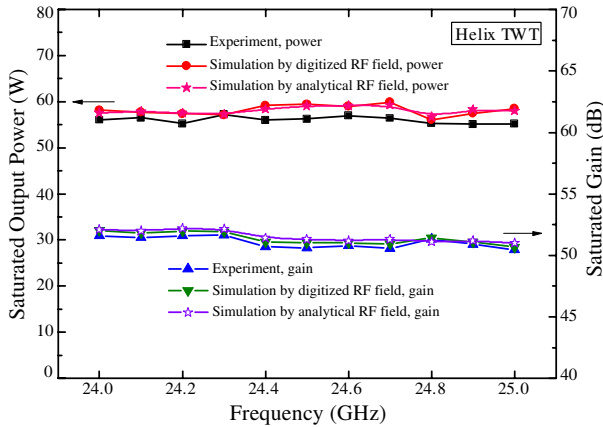


Figure 7. Comparison of the saturated output power and gain between the experimental and simulation results for the helix TWTA over the bandwidth.

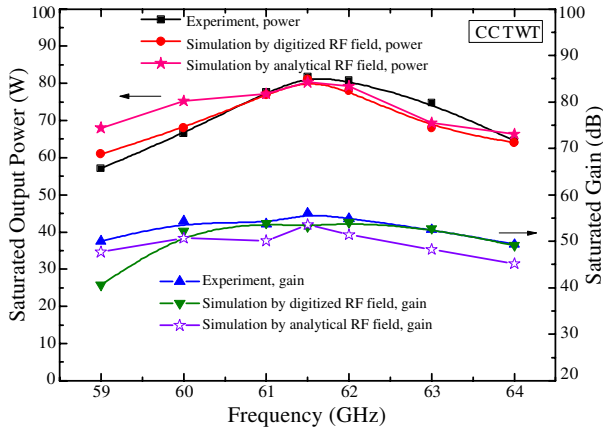


Figure 8. Comparison of the saturated output power and gain between the experimental and simulation results for the CC TWTA over the bandwidth.

theories are consistent, too.

Figure 9 shows that for the FWG TWTA, the average relative error over the bandwidth for the saturated output power is 4.2%, and for the saturated gain, the corresponding value is 1.6%. There are mainly two reasons for the wide difference between the experimental and simulated curves for the FWG TWTA. First, in the 1-D model, the transverse effect from the non-axial symmetric nature of SWS in

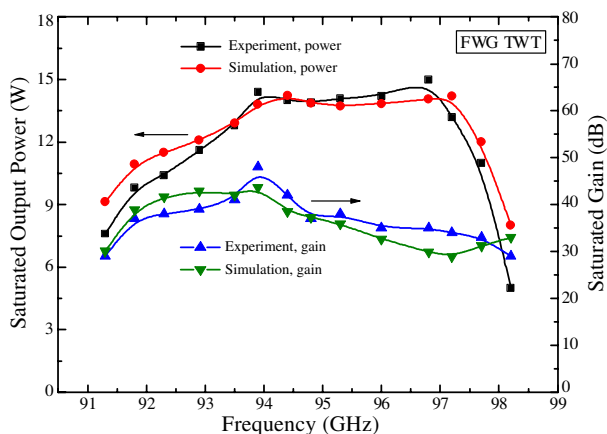


Figure 9. Comparison of the saturated output power and gain between the experimental and simulation results for the FWG TWTA over the bandwidth.

this FWG TWTA is not included. Second, the smaller size of the SWS in the W-band TWTA makes it more sensitive to manufacturing technologies than the other two TWTAs.

It can be concluded that saturated output power and gain curves for the helix, CC, FWG TWTAs can be accurately predicted. This nonlinear theory is validated by the consistent comparison between the simulated and experimental results. However, a multi-dimensional model of this digitized nonlinear theory should be developed in the future, because it would be more useful to engineers. The RF field profiles on transversal grids need to be considered and the outer focus magnetic fields need to be included. Additionally the electron beam will be treated as charge rings or beamlets [7] to account for their transversal trajectories.

4. CONCLUSION

A digitized nonlinear theory for the BWI of TWTAs has been presented in this paper. This theory can be applied in various types of TWTAs. A K-band helix TWTA, a V-band CC TWTA, and a W-band FWG TWTA are simulated by the corresponding 1-D code which shows good predictions when comparing its simulation output power and gain curves with the experimental tests. For further simulation, the multi-dimensional code, as well as the BWI theory within the backward wave oscillation (BWO) and reflections will be included in our future research.

ACKNOWLEDGMENT

This work was supported by the National Natural Science Foundation of China (Grant Nos. 61201003, 60931001, 61071030 and 10905009). The authors would like to express gratitude to Professors Yan-Mei Wang, Jin-Jun Feng, Yin-Fu Hu and Xian-Ping Wu in Beijing Vacuum Electronics Research Institute for the experimental tests of the helix and the FWG TWTAs. We also express gratitude to Mike M. Clark at the Department of Physics, University of Wisconsin, Madison, Wisconsin, the USA, for helping with English grammar.

REFERENCES

1. Pierce, J. R., *Traveling Wave Tubes*, D. Van Nostrand, New York, 1950.
2. Rowe, J. E., *Nonlinear Electron-Wave Interaction Phenomena*, Academic Press, Inc., New York, 1965.
3. Pierce, J. R. and L. M. Field, "Traveling-wave tubes," *Proc. IRE*, Vol. 35, 108–111, 1947.
4. Rowe, J. E., "A large-signal analysis of the traveling-wave amplifier: Theory and general results," *IEEE Trans. Electron Dev.*, Vol. 3, No. 1, 39–56, 1956.
5. Antonsen, Jr., T. M., A. A. Mondelli, B. Levush, J. P. Verboncoeur, and C. K. Birdsall, "Advances in modeling and simulation of vacuum electronic devices," *Proc. IEEE*, Vol. 87, No. 5, 804–839, 1999.
6. Antonsen, Jr., T. M. and B. Levush, "Traveling-wave tube devices with nonlinear dielectric elements," *IEEE Trans. Plasma Sci.*, Vol. 26, No. 3, 774–786, 1998.
7. Chernin, D. P., T. M. Antonsen, Jr., B. Levush, and D. R. Whaley, "A three-dimensional multifrequency large signal model for helix traveling wave tubes," *IEEE Trans. Electron Dev.*, Vol. 48, No. 3, 3–11, 2001.
8. Freund, H. P., E. G. Zaidman, and T. M. Antonsen, Jr., "Theory of helix traveling wave tubes with dielectric and vane loading," *Phys. of Plasmas*, Vol. 3, No. 8, 3145–3161, 1996.
9. Freund, H. P. and E. G. Zaidman, "Nonlinear theory of collective effects in helix traveling wave tubes," *Phys. of Plasmas*, Vol. 4, No. 6, 2292–2301, 1997.
10. Freund, H. P. and E. G. Zaidman, "Time-dependent simulation of helix traveling wave tubes," *Phys. of Plasmas*, Vol. 7, No. 12, 5182–5194, 2000.

11. Srivastava, V., "SUNRAY-2.5D code for multi-signal large-signal analysis of a complete helix TWT," *IEEE Int. Vacuum Electron. Conf.*, 303–304, Bangalore, India, 2011.
12. Chernin, D. P., D. Dialetis, T. M. Antonsen, Jr., J. Legarra, J. Qiu, and B. Levush, "Validation studies for CHRISTINE-CC using a Ka-band coupled-cavity TWT," *IEEE Int. Vacuum Electron. Conf.*, 399–400, Monterey, California, 2006.
13. Chernin, D. P., T. M. Antonsen, Jr., I. A. Chernyavskiy, A. N. Vlasov, B. Levush, R. Begum, and J. R. Legarra, "Large-signal multifrequency simulation of coupled-cavity TWTs," *IEEE Trans. Electron Dev.*, Vol. 58, No. 4, 1229–1239, 2011.
14. Freund, H. P., T. M. Antonsen, Jr., E. G. Zaidman, B. Levush, and J. Legarra, "Nonlinear time-domain analysis of coupled-cavity traveling-wave tubes," *IEEE Trans. Plasma Sci.*, Vol. 30, No. 3, 1024–1040, 2002.
15. Wallander, S. O., "Large signal analytical study of bunching in klystrons," *IEEE Trans. Electron Dev.*, Vol. 15, No. 8, 595–603, Aug. 1968.
16. Morwood, R. C. and F. I. Friedlander, "LSCEX3: A computer program for large signal analysis of klystrons, twystrons, and traveling wave tubes with cavity circuits," Varian Associates Report, Dec. 1979.
17. Vaughan, J. R., "Calculation of coupled-cavity TWT performance," *IEEE Trans. Electron Dev.*, Vol. 22, No. 10, 880–890, Oct. 1975.
18. Vlasov, A. N., T. M. Antonsen, Jr., D. P. Chernin, B. Levush, and E. L. Wright, "Simulation of microwave devices with external cavities using MAGY," *IEEE Trans. Plasma Sci.*, Vol. 30, No. 3, 1277–1291, 2002.
19. Vlasov, A. N., S. J. Cooke, B. Levush, T. M. Antonsen, Jr., I. A. Chernyavskiy, and D. Chernin, "Modeling of coupled cavity TWT with TESLA," *Proc. Int. Conf. Vacuum Electron.*, 155–156, Rome, Italy, 2009.
20. Vlasov, A. N., S. J. Cooke, B. Levush, T. M. Antonsen, Jr., I. A. Chernyavskiy, and D. Chernin, "2D modeling of beam-wave interaction in coupled cavity TWTs with TESLA," *Proc. Int. Conf. Vacuum Electron.*, 405–406, Monterey, CA, 2010.
21. Goplen, B., L. Ludeking, D. Smithe, and G. Warren, "User configurable MAGIC code for electromagnetic PIC calculations," *Comput. Phys. Commun.*, Vol. 87, Nos. 1–2, 54–86, 1995.
22. Ansoft HFSS, 3-D electromagnetic Simulation Software, Ansoft

- Corp., Pittsburgh.
23. Wilson, J. D. and C. L. Kory, "Simulation of cold-test parameters and RF output power for a coupled-cavity traveling-wave tube," *IEEE Trans. Electron Dev.*, Vol. 42, No. 11, 2015–2020, 1995.
 24. Hu, Y. F., J. J. Feng, J. Cai, Y. H. Du, Y. Tang, and X. P. Wu, "Performance enhancement of W-band CW TWT," *IEEE Int. Vacuum Electron. Conf.*, 21–22, Bangalore, India, 2011.
 25. Morey, I. J. and C. K. Birdsall, "Traveling-wave-tube simulation: The IBC code," *IEEE Trans. Plasma Sci.*, Vol. 18, No. 3, 482–489, 1990.
 26. Booske, J. H., M. C. Converse, C. K. Kory, C. T. Chevalier, D. A. Gallagher, K. E. Kreischer, V. O. Heinen, and S. Bhattacharjee, "Accurate parametric modeling of folded waveguide circuits for millimeter-wave traveling wave tubes," *IEEE Trans. Electron Dev.*, Vol. 52, No. 5, 685–694, 2005.
 27. Bernardi, P., F. André, J. F. David, A. L. Clair, and F. Doveil, "Efficient time-domain simulations of a helix traveling-wave tube," *IEEE Trans. Electron Dev.*, Vol. 58, No. 6, 1716–1767, 2011.
 28. Freund, H. P., "Nonlinear theory of helix traveling wave tubes in the frequency domain," *Phys. of Plasmas*, Vol. 6, No. 9, 3633–3646, 1999.
 29. Hou, Y., J. Xu, H. R. Gong, Y. Y. Wei, L. N. Yue, G. Zhao, and Y. B. Gong, "Equivalent circuit analysis of ridge-loaded folded-waveguide slow-wave structures for millimeter-wave traveling-wave tubes," *Progress In Electromagnetics Research*, Vol. 129, 215–229, 2012.
 30. Liu, Y., J. Xu, Y.-Y. Wei, X. Xu, F. Shen, M. Huang, T. Tang, W.-X. Wang, Y.-B. Gong, and J. Feng, "Design of a v-band high-power sheet-beam coupled-cavity traveling-wave tube," *Progress In Electromagnetics Research*, Vol. 123, 31–45, 2012.
 31. Li, B., Z. H. Yang, J. Q. Li, X. F. Zhu, T. Huang, X. L. Jin, Q. Hu, Y. L. Hu, L. Xu, J. J. Ma, L. Liao, L. Xiao, and G. X. He, "Theory and design of microwave-tube simulator suite," *IEEE Trans. Electron Dev.*, Vol. 56, No. 5, 919–927, 2009.
 32. Bai, C. J., J. Q. Li, Y. L. Hu, Z. H. Yang, and B. Li, "A nonlinear theory for coupled-cavity TWTs in beam-wave interaction," *Int. Conf. Microwave and Millimeter Wave Tech.*, Vol. 5, 1–4, Chengdu, China, 2012.